

On the possibility that STS “gap-maps” of cuprate single crystals are dominated by \mathbf{k} space anisotropy and not by nano-scale inhomogeneity.

J.R. Cooper

Department of Physics, University of Cambridge,

J. J. Thomson Avenue, Cambridge CB3 OHE, U.K.*

(Dated: October 22, 2018)

The results of a computer analysis of a simple 2D quantum mechanical tunnelling model are reported. These suggest that the spatial dependence of the superconducting energy gap observed by Scanning Tunnelling Spectroscopy (STS) studies of single crystals of the high T_c superconductor $\text{Bi}_2\text{Sr}_2\text{CaCu}_2\text{O}_{8+x}$ is not necessarily caused by nanoscale inhomogeneity. Instead the spatial dependence of the STS data could arise from the momentum (\mathbf{k}) dependence of the energy gap, which is a defining feature of a d -wave superconductor. It is possible that this viewpoint could be exploited to obtain \mathbf{k} dependent information from STS studies.

I. INTRODUCTION

In recent scanning tunnelling spectroscopy (STS) experiments, differential conductance ($G \equiv dI/dV$) versus voltage (V) curves are measured at many thousands of points on the surface of single crystals of the highly anisotropic cuprate superconductor $\text{Bi}_2\text{Sr}_2\text{CaCu}_2\text{O}_{8+x}$ or Bi:2212^{1,2}. The form of $G(V)$ at every point is roughly that expected from a tunnel junction between a normal metal and a d -wave superconductor. However, the superconducting gap parameter, Δ , determined from the peaks in $G(V)$, varies strongly and continuously with position, from 20 to 70 meV with a typical length scale of 1–2 nm. It is thought that $G(V)$ is a direct measure of the local quasi-particle density of states (DOS) and therefore these “gap maps” are widely accepted as being associated with nanoscale inhomogeneity, implying that the superconducting gap and all other superconducting properties are spatially inhomogeneous. It is difficult to reconcile this picture with the results of other experiments such as NMR³ and heat capacity⁴, where such gross inhomogeneity is not detected.

The energy (E) dependent quasi-particle DOS, $N(E)$ in a d -wave superconductor with a \mathbf{k} -dependent order parameter $\Delta(\mathbf{k})$ can be thought of as the sum of s -wave like contributions from different directions in \mathbf{k} -space, i.e., $N(E) = \frac{2}{(2\pi)^3} \int \frac{dS}{\hbar|v(\mathbf{k})|} \frac{E}{[E^2 - \Delta(\mathbf{k})^2]^{1/2}}$, where dS is a small element of a constant energy surface in the normal state with electron velocity $v(\mathbf{k})$. The measured quantity $G(V)$ is proportional to $\frac{2}{(2\pi)^3} \int dE \int \frac{dS}{\hbar|v(\mathbf{k})|} P(\mathbf{k}) \frac{E\delta(E-V)}{[E^2 - \Delta(\mathbf{k})^2]^{1/2}}$, where $P(\mathbf{k})$ is the probability of tunnelling into a state \mathbf{k} , so $G(V)$ only reflects the behavior of $N(E)$ precisely when $P(\mathbf{k})$ is constant. For a defect-free *planar* metal-insulator-superconductor tunnel junction, transverse momentum (\mathbf{k}_T) will be conserved because of translational invariance. Also, because of the exponential decay of the evanescent wave in the barrier, the tunnelling current will be dominated by states with smaller values of $|\mathbf{k}_T|$, that lie within a “tunnelling cone” whose angular width depends on the strength and width of the barrier⁵. So, for *planar* tunnelling into a superconductor with a

reasonably large Fermi surface, $P(\mathbf{k})$ is not constant, because final states with larger values of $|\mathbf{k}_T|$ will not be accessible. But for planar tunnelling perpendicular to the conducting layers of a quasi-2D material such as Bi:2212, $P(\mathbf{k})$ is constant if the quasi-2D Fermi surface is electron-like and exactly circular⁶, or if the “tunnelling cone” is wide enough, i.e. $|\mathbf{k}_T|$ is large enough, so that P does not vary much over the Fermi surface⁶. At first sight, spatial confinement of the initial electron states in the sharp STS tip would be expected to give a larger spread in \mathbf{k}_T , so there would be an even greater tendency for P to be constant for *c*-axis tunnelling into Bi:2212 using STS. This seems to be the prevailing view in the field. While the model calculations reported here do show that for realistic STS tip sizes and tip materials, \mathbf{k}_T is not conserved, i.e. there is no well-defined refracted wave in the quasi-2D metal, they also show that P is not constant. Instead it falls drastically as the in-plane wave number of Bi:2212, represented by the parameter $|k_y|$ in the model, is increased.

Recent STS studies give clear experimental evidence that bigger gaps are observed in areas of the crystal where there are more off-stoichiometric oxygen atoms in the BiO-SrO layer². In a naive semi-classical picture these O^{2-} ions would scatter the tunnelling electrons, via the Coulomb interaction, giving them extra transverse momentum. So there could be a tendency for a particular in-plane direction of \mathbf{k} to have extra weight in $G(V)$ at a certain separation between the STS tip and an O^{2-} ion and hence a particular value of $\Delta(\mathbf{k})$ could be favored there. This provides a mechanism for variations in the peaks in $G(V)$ as the STS tip is moved across the surface of the crystal without invoking nanoscale inhomogeneity.

The model calculations reported here are consistent with this semi-classical picture in that the strong k_y dependence of P mentioned above becomes much less marked when there are O^{2-} ions near the STS tip. Although they do not give a completely adequate description of the observed $G(V)$ curves, they seem to capture the important physics and future microscopic calculations of the $G(V)$ curves should take the present results into account.

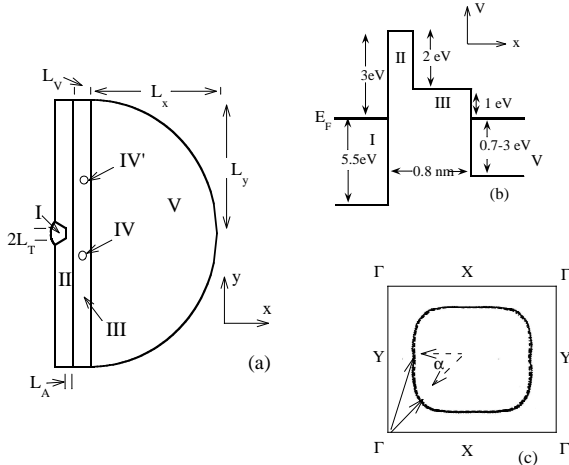


FIG. 1: (a) Spatial regions used for 2D tunnelling calculations, I STS tip, II vacuum, III BiO-SrO layer, IV and IV' oxygen ions, V Bi:2212. (b) Corresponding potential energies versus distance (x) at $y = 0$. (c) Typical Fermi surface cross-section⁷, with solid arrows marking the minimum and maximum \mathbf{k} vectors considered here and dashed arrows showing the angle α with the $(-\pi, 0)$ direction (see text).

II. THE MODEL

The spatial dimensions and energy barriers of the 2D quantum mechanical tunnelling model are defined in Figures 1(a) and 1(b) respectively. Region I corresponds to the STS tip, which is the projection of a truncated cone with sides at 30 degrees to the surface normal, i.e. to the c -axis of the cuprate crystal. The Fermi energy of 5.5 eV in the tip corresponds to a free electron wave vector of 12 nm^{-1} which is close to the Fermi wave vector (k_F^{Au}) of typical tip materials such as Au or a Pt alloy. The vacuum gap in region II was generally taken to have a width $L_A = 0.24 \text{ nm}$ and a barrier height of 3 eV as deduced from STS work⁸. The boundary condition on the small line of length $2L_T$ represents an incoming electron wave of the form $\exp[ik_F^{Au}(x \cos \theta + y \sin \theta)]$ travelling at an angle θ to the normal, i.e. on this line (where $x=0$) the real and imaginary parts of the wave function, ψ_R and ψ_I were set equal to $\cos(k_F^{Au}y \sin \theta)$ and $\sin(k_F^{Au}y \sin \theta)$ respectively. The STS tip width $2L_T$ was often fixed at 0.3 nm but calculations were made for a range of values between 0.15 and 5 nm. For $2L_T = 5 \text{ nm}$ (i.e. 10 times the wavelength of the electrons in the Au tip) the result expected for a planar junction, namely conservation of transverse momentum was obtained. However for $2L_T \leq 0.6 \text{ nm}$ there was no evidence for \mathbf{k}_T conservation, i.e. no sign of a wave propagating at the appropriate angle in region V. The angle θ was varied between 0 and 30 degrees, but since the number of initial states in the tip increases as $\sin \theta$, Ref. 5, it was decided that 25 degrees was appropriate for comparison with experiment. This choice does not affect our conclusions.

Region III corresponds to the BiO-SrO layer which is

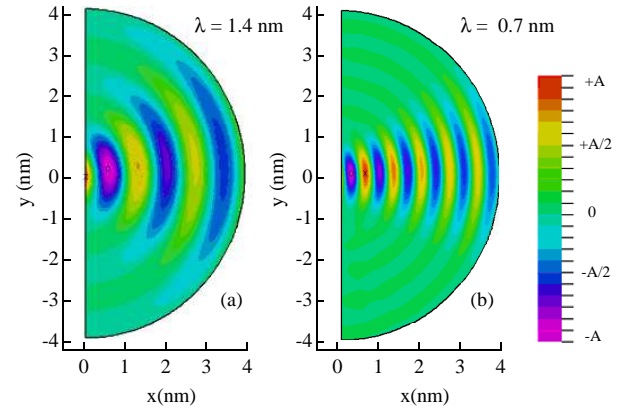


FIG. 2: (Color on-line). Contour plots in the (x, y) plane of real part of wave function ψ_R in region V for wavelengths of (a) 1.4 nm and (b) 0.7 nm , using the parameters given in Fig. 1(b) and without any O^{2-} ions. Here x is measured from the start of region V. The linear color scale is also shown.

taken to be 0.56 nm wide⁹. In most of the calculations a barrier height of 1 eV, consistent with band theory⁷, was used. This layer is now believed to be insulating in view of (a) the extremely large and non-metallic c -axis resistivity of Bi:2212 crystals¹⁰ and (b) various experiments on intrinsic c -axis tunnelling in mesa structures, for example Ref. 11. Region V, where the potential energy $V(x, y)$ is constant, corresponds to the bulk of the cuprate superconductor. Representing the electronic structure of the cuprates by a free electron model, which is effectively done here, is a drastic approximation. However including an extra barrier to represent the c -axis lattice potential, i.e. the next BiO-SrO layer, does not alter the main conclusions because a defect-free planar barrier would reflect semi-circular waves such as those shown in Figure 2 without altering k_y . This point was checked explicitly by introducing an appropriate extra planar barrier in region V. This had no effect on the behavior shown later for $P(k_y)$ in the absence of O^{2-} ions, but because of standing waves there was more scatter in the results.

The present model is therefore a useful starting point for discussing the effect of oxygen ions in the barrier layer and for discussing whether the STS technique does indeed give a true \mathbf{k} -space average of the electronic DOS. The value of the Fermi energy E_F in region V was varied over the range 0.76 to 3.04 eV because this corresponds to free electron wave numbers from 4.47 to 8.94 nm^{-1} and wavelengths between 1.4 and 0.7 nm. These wave numbers are approximately equal to the minimum and maximum in-plane values of k_F for electron states at the Fermi energy in the cuprates shown in Figure 1(c). In tunnelling problems one always considers the “physical electron” as emphasized by Anderson in connection with inter-layer tunnelling in the cuprates.

The small circular regions IV and IV' in Figure 1(a) correspond to spherically symmetric O^{2-} ions with a full outer shell situated 0.1 nm from the CuO_2 layer. They

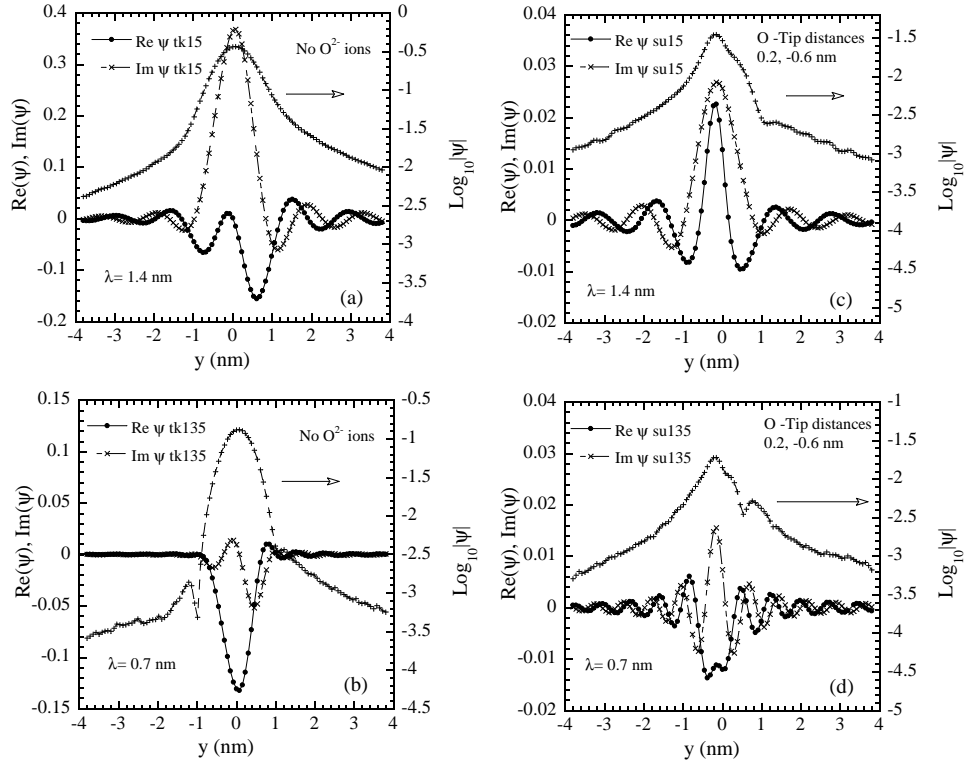


FIG. 3: Plots of the electron wave function (ψ_R , ψ_I and $|\psi|$) in a narrow strip of width $x = 0.05$ nm extending from $y = -3.8$ to 3.8 nm, just inside region V, i.e. the first CuO_2 layer. Computed data for the two limiting wavelengths are shown in (a) and (b) in the absence of O^{2-} ions and in (c) and (d) with O^{2-} ions at $+0.2$ and -0.6 nm from the center of the STS tip. Parameter values are those in Figure 1 (b), with $2L_T = 0.3$ nm, $L_A = 0.24$ nm and θ (see text) = 25 degrees.

give rise to a Coulomb field outside a typical atomic radius of 0.06 nm. In the metallic region V, this field will be strongly screened by the mobile electrons (on a length scale of order k_F^{-1}). As often done in tunnelling problems¹⁵ this screening is represented by an equal and opposite image charge in region V giving a dipole field from each non-stoichiometric O^{2-} ion in the BiO-SrO layer. For simplicity, dielectric screening in the BiO-SrO layer is ignored since positive polarization charges at the II-III boundary can then be neglected. However in order to compare with experiments, where the mean spacing between O^{2-} ions is typically 0.8 nm, the Coulomb field was multiplied by a Gaussian attenuation factor, $\exp(-(y - y_1)^2/\sigma^2)$ where y_1 is the y co-ordinate of the O^{2-} ion and $\sigma = 0.4$ nm. This was done because the tunnelling electrons will be scattered by *local* increases in the Coulomb potential above a uniform background potential given by more distant O^{2-} ions. The Coulomb potential inside region IV was set equal to a constant, namely its value at the III-IV boundary. For simplicity it was also assumed that the dipole electric field does not extend into the vacuum region II or into the metallic region V.

III. METHOD AND RESULTS

A commercially available partial differential equation (PDE) PC package¹² was used to solve the 2D Schrödinger equations for ψ_R and ψ_I with the above potentials. An example program attributed to Backstrom¹² and initial tests for the textbook problem of tunnelling through a 1D potential barrier¹³ were helpful in setting the boundary conditions (BCs), details of which are given in footnote 14. The BCs on the semicircular bounding surfaces shown in Figure 1(a) were chosen so that outwardly propagating waves are favored and the absence of significant standing waves was verified by comparing plots of $|\psi|$ and ψ_R along various lines in region V. Most of the calculations were done for the geometry shown in Figure 1(a) with $L_x = L_y = 4$ nm but checks were made for larger values of L_x , for a rectangular bounding region and also for a cylindrically symmetric 3D case. The graphical output given by the PDE program was typically in the form of contour plots of ψ_R such as those in Figures 2(a) and (b) or plots of ψ_R and $\log|\psi|$ along certain lines (not shown). Arrays of 101×101 ψ_R and ψ_I values over various user-defined regions of Figure 1(a) were also generated and these were processed further using other commercially available PC packages.

Figures 2(a) and (b) show examples of the contour

plots for the two extreme k_F values mentioned above in the absence of any impurities in the barrier. Note that the shorter wavelength waves are more concentrated in the forward direction. As justified in detail later, this leads to the key result of the present work, namely $P(k_y)$ is not constant for tunnelling between a sharp STS tip and Bi:2212 and therefore the $G(V)$ curves will give a distorted image of the DOS. The barriers are relatively weak so that the width of the “source” along y just inside region V is considerably wider than that of the STS tip (0.3 nm). For the parameters given in Figure 1(b) and used in Figure 2, the regions of high intensity below the STS tip and 0.2 nm inside the conducting region V have FWHM in $|\psi|$, of $\delta y = 1.16$ nm and 0.84 nm, for $\lambda = 1.4$ and 0.7 nm respectively. The ratios $\lambda/\delta y$ differ by a factor 1.5 and this, together with the fact that $\lambda \simeq \delta y$ and δx , must be responsible for difference in spreading out of the waves shown Figures 2(a) and 2(b). Another important point is that, as mentioned in the previous section, there is little asymmetry between positive and negative y values, despite the fact that the wave coming in to the STS tip is at 25 degrees to the surface normal, and therefore has significant transverse momentum $k_y = k_F^{Au} \sin(25) = 5.1 \text{ nm}^{-1}$ along y . In contrast to the planar tunnelling case, no refracted wave that conserves k_y is produced because the STS tip width, $2L_T = 0.3$ nm is too small, as shown later in Figure 4(c).

Computed data are shown in more detail in Figures 3(a) to 3(d) as plots of ψ_R , ψ_I and $\log|\psi|$ versus y at a mean distance along x of 0.25 nm into region V. The data shown are in fact the sum of 100 ψ values between $x = 0$ and 0.5 nm, now measured from the beginning of region V, for fixed values of y . A strip of this width corresponds to the first CuO_2 bi-layer in Bi:2212,⁹ but the same results are obtained for different strips e.g. between $x = 0$ and 0.3 nm. The $|\psi|$ plots are shown on a semi-logarithmic scale in order to see the behavior at larger values of y . There are no significant oscillations in $|\psi|$ showing that the BCs do indeed produce propagating and not standing waves. The periods of the oscillations in ψ_R and ψ_I along y are very close to the two wavelengths used, 0.7 and 1.4 nm. Figures 3(a) and 3(b) show data with no O^{2-} ions in the BiO-SrO layer. Comparison of the two figures shows that the shorter wavelength has lower amplitude oscillations, by at least a factor 10, over most of the range of y confirming the differences shown in Figures 2(a) and 2(b). Figures 3(c) and 3(d) show the effect of having one O^{2-} ion at $y = +0.2$ nm and another at $y = -0.6$ nm, a spacing typically observed in the experiments², the center of the STS tip being at $y = 0$. The key point is that in the presence of O^{2-} ions the amplitude is much less dependent on the wavelength. This suggests that STS does not give a true DOS average for quasi-2D superconductors and that the presence of O^{2-} ions allows states with larger values of k_y to be accessed.

IV. COMPARISON WITH EXPERIMENT

In order to make an initial comparison with experiment the following procedure was used. The $\psi(y)$ data such as those shown in Figures 3(a) to 3(d) were multiplied by $\exp(-i2\pi y/\lambda)$ or $\exp(i2\pi y/\lambda)$ and integrated over y to give the (complex) numbers $a(k_y)$ and $a(-k_y)$. These are the quantum mechanical overlap integrals between an initial electron state in the STS tip and plane waves of wavelength λ propagating in the $\pm y$ directions in region V. Hence the quantity $|a(k_y)|^2 + |a(-k_y)|^2$ is the required probability $P(k_y)$ of electron tunnelling from the tip into a state in region V with $|k_y| = 2\pi/\lambda$. $P(k_y)$ was calculated for a range of λ values between 1.4 and 0.7 nm. Since the Schrödinger equation is linear in ψ and the solutions are obtained by matching ψ and $\nabla\psi$ at the boundaries it is plausible, but not proved, that the same probability function $P(k_y)$ would also apply to the physically realistic case of the Bi:2212 bands where, as shown in Figure 1(c), there is a range of $|\mathbf{k}|$ values with the same (Fermi) energy. Typical behavior of $P(k_y)$ is shown in Figures 4(a) and 4(b) for various positions of the STS tip relative to one or two O^{2-} ions respectively. Generally P varies as $A \exp(-B|k_y|)$, where A and B are constants, but especially when the spacing of the two ions is $\sim \lambda$, there is some extra curvature in plots of $\log P$ vs. k_y which probably arises from two-beam interference effects. As shown by the curve *ta* in Figure 4(b), two nearby O^{2-} ions reduce P by 2-3 orders of magnitude, this is understandable because the height of the BiO-SrO barrier is increased locally from 1 eV to approximately 5 eV. Figure 4(c) shows the behavior of $P(k_y)$ for different STS tip widths ($2L_T$) ranging from 0.15 to 3 nm in the absence of O^{2-} ions. The exponential behavior mentioned above persists up to $2L_T = 0.6$ nm, after which there is a sharper fall associated with the tendency towards conservation of k_y for a planar junction.

These $P(k_y)$ values were then used to calculate the corresponding $G(V)$ curves expected in the superconducting state. Referring back to Figure 1(c), the contribution to $G(V)$ from a \mathbf{k} -vector on the Fermi surface was weighted by $P(|\mathbf{k}|)$ where $|\mathbf{k}|$ is the distance from the Γ point. Because of the simplicity of the model, calculations were limited to the region between the two solid arrows in Figure 1(c). The behavior of $P(k_y)$ for different O^{2-} environments shown in Figures 4(a) and (b) means that small gap regions near the d -wave nodes are heavily favored in the absence of O^{2-} ions but that scattering from O^{2-} ions allows higher gap regions to be accessed. Figure 4(d) shows that this conclusion is not strongly dependent on parameter values such as the STS tip width $2L_T$, the BiO-SrO barrier height or the spacing between the STS tip and the Bi:2212 surface (L_A). Some typical calculated $G(V)$ curves are shown as un-normalized plots in Figure 5(a) and as normalized ones in Figure 5(b). In generating these curves the standard weak-coupling d -wave form for the gap parameter, $\Delta(\mathbf{k}) = \Delta \cos(2\alpha)$ was used, where α is the angle between \mathbf{k} and the $(-\pi, 0)$ direction shown

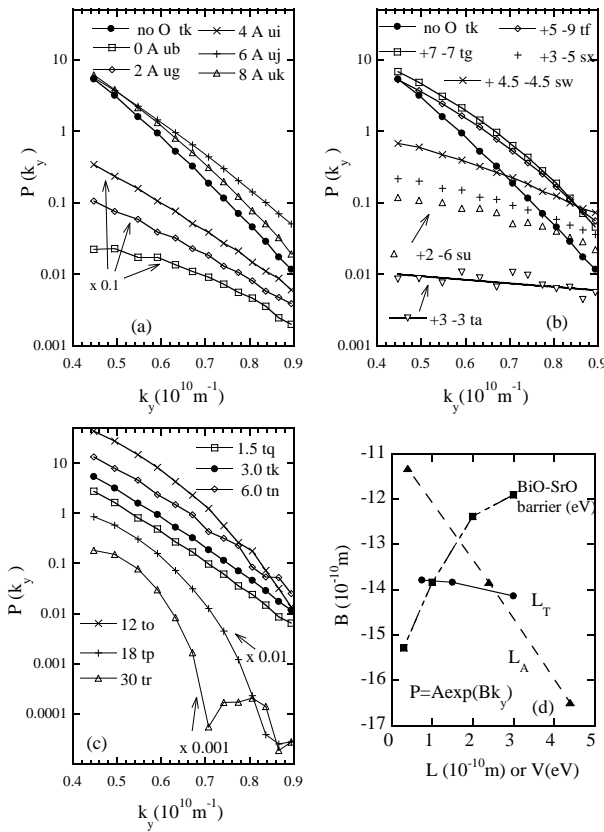


FIG. 4: Plots of $P(k_y)$, the probability weighting factor (see text) versus k_y , (a) with no O^{2-} ions present (solid black circles) and with one ion present at different distances, in A° units (0.1nm) from the STS tip. (b) with pairs of ions at different distances, in A° , and (c) with no ions present but for various tip widths, $2L_T$ in A° . (d) Effect of various parameters, the BiO-SrO barrier height in eV, the vacuum gap L_A in A° , and the STS tip half-width L_T on the mean slope of $\log_e(P)$ vs. k_y in the absence of O^{2-} ions.

by dashed arrows in Figure 1(c). Tunnelling data invariably show some broadening of the $G(V)$ curves that is ascribed to a finite quasi-particle lifetime (\hbar/Γ). In the Dynes formula¹⁶ used by Wei et al.⁶ E is replaced by $E - i\Gamma$ and $N(E)$ is given by the real part of the usual expression. This formula should not be applied when $\Gamma \sim \Delta$ ¹⁶ and therefore, in the present calculations, moderate damping, namely $\Gamma = 0.1\Delta(\mathbf{k})$ was assumed for all \mathbf{k} . In future it might be possible to derive experimental values of $\Gamma(E, \mathbf{k})$ by appropriate fits to the STS $G(V)$ curves.

V. DISCUSSION

The un-normalized $G(V)$ curves shown in Figure 5(a) are similar to some of the published experimental data, e.g. the first paper by Pan et al.¹⁷ where there is clearly a strong reduction in the magnitude of $G(V)$ in the regions

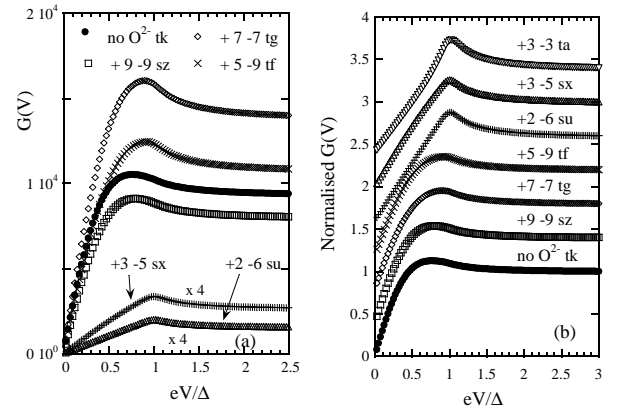


FIG. 5: (a) Calculated $G(V)$ curves for a d -wave DOS in the same (arbitrary) units plotted versus eV/Δ for no O^{2-} ions, curve tk , and pairs of O^{2-} ions at various distances, y in A° , from the STS tip at $y = 0$. (b) Corresponding $G(V)$ curves normalized to unity at $eV = 3\Delta$ and displaced vertically by multiples of 0.4.

where the gap appears to be larger. It also noteworthy that curves labelled tk , tg , tf and sz seem to show very similar behavior at low voltages a feature that is also present in the experimental data, for example Figure 3 of Ref. 1. The peaks in $G(V)$ vary from $V = 0.7\Delta/e$ to Δ/e . However even though $P(k_y)$ varies drastically with k_y when there is little scattering by the O^{2-} ions, the corresponding $G(V)$ curves do appear to be more rounded than those observed experimentally, especially recently^{2,18}.

Within the present approach even higher \mathbf{k} - space selectivity may be needed to account for the experimental STS data. There are several ways in which this might occur. Firstly in the present model the band-structure of the BiO-SrO layer is ignored. In a microscopic treatment one would consider tunnelling to arise from virtual excitations into the BiO-SrO conduction band. This band is likely to have a narrow energy width and hence for a given impact parameter the transverse momentum gained by scattering from an O^{2-} ion may well be better defined than in the present model. Secondly the band structure of the CuO_2 layer is not included. Since this is a tight binding band structure, Fermi surface states nearer the Brillouin zone boundary, i.e. those with small values of the angle α in Figure 1(c), will contain significant components of states with higher momenta, namely $\mathbf{k} + \mathbf{G}$ where \mathbf{G} is a reciprocal lattice vector. This will give even less weight to the states with higher values of $|\mathbf{k}|$.

Thirdly the standard “semiconductor model” is used to describe the tunnelling DOS of a superconductor. The theory of Blonder, Klapwijk and Tinkham (BTK)¹⁹, which makes use of the Bogoliubov equations rather than the Schrödinger equation, often provides good fits to $G(V)$ curves of superconductors obtained with either metallic point contacts or small-area tunnel junctions, despite fact that it uses a 1D model. BTK theory con-

tains some features that could be relevant here, for example the quasi-particle current transforms into a supercurrent over the coherence length which in the present case is highly \mathbf{k} -dependent. A paper²⁰ applying BTK theory to a *d*-wave superconductor does conclude that $G(V) \sim N(V)$, but because a 1D model is used, \mathbf{k}_T is conserved, in contrast to the present work.

Fourthly, the presence of a pseudogap would also reduce or eliminate contributions to $G(V)$ from the regions of the Fermi surface with larger values of $|\mathbf{k}|$. In a model used to account for heat capacity data²² there is a triangular non-states-conserving pseudogap that ARPES experiments, e.g. Refs. 23 and 24, suggest has greatest effect in the anti-nodal directions. Introduction of a pseudogap would help in fitting the V-shaped, apparently non-states-conserving $G(V)$ curves that are often observed experimentally by STS^{2,17,18,21}. Reports from other STS groups^{21,25,26} suggesting that, especially for overdoped Bi:2212 crystals, the normalized $G(V)$ curves can be uniform for linear scans over 10 – 20 nm do not necessarily contradict the picture presented here, since as shown in Figs. 4(a), 4(b) and 5(b) the normalized $P(k_y)$ curves and hence the normalized $G(V)$ curves, can be quite similar for a variety of O^{2-} spacings.

Finally and perhaps most importantly, the \mathbf{k} -selectivity could be further increased by the interference of scattered waves from different O^{2-} ions. There are some indications of this effect in the $P(k_y)$ curve labelled *tg* in Figure 4(b) where the STS tip is placed symmetrically between two ions at a distance $\sim \lambda$ from each. These effects could well be more marked in the realistic 3D case where “multiple beam” interference is more likely, for example the scattered waves from 3 or 4 suitably spaced O^{2-} ions could interfere constructively for certain directions of \mathbf{k} to give 9 or 16 times higher intensity. Since the positions of the O^{2-} ions can be found using STS² it might even be possible to locate such structures and hence obtain better \mathbf{k} -resolution in the experiments. A faster PDE program would be needed to investigate these 3D aspects using the present model. However the main result reported here, namely the strong variation of P with k_y in the absence of O^{2-} ions and the weaker dependence in their presence has been verified for one special 3D case. This is the cylindrically

symmetric situation where the O^{2-} ion is positioned immediately below the STS tip and the electron wave comes in at normal incidence.

VI. SUMMARY AND CONCLUSIONS

A new way of interpreting the “gap-maps” observed in STS studies of cuprate superconductors has been proposed that does not invoke nanoscale inhomogeneity. In principle, perhaps when extended to include real atomic orbitals and band structure, it can be used to obtain \mathbf{k} -resolved information from STS data.

Note added on 26th Jan. 2007. Since submitting this paper I became aware of analytical theory²⁷ of the scanning tunnelling microscope for a spherical STS tip. Equations (4) and (9) of Ref. 27 lead to results that are consistent with the present work for a single barrier without any O^{2-} ions. Neglecting terms with reciprocal lattice vectors, $\vec{G} \neq 0$, gives a tunnelling probability $P \propto \exp[-2(\kappa^2 + |\vec{k}_{||}|^2)^{1/2}|\vec{r}_0|]$, where²⁷ $\kappa = \hbar^{-1}(2m\phi)^{1/2}$ is the minimum inverse decay length, $\vec{k}_{||}$ the in-plane electron wave-number, ϕ the work function (i.e. the barrier height relative to E_F) and \vec{r}_0 the distance between the center of curvature of the STS tip and the sample surface. For a barrier height of 3 eV and $|\vec{r}_0| = 0.8$ nm, fitting the above formula to $P = A \exp(Bk_y)$ over the range of $k_y (\equiv \vec{k}_{||})$ used here gives $B = -9.6 \cdot 10^{-10} \text{ m}^{-1}$. Bearing in mind that the present calculations were made for a flat STS tip and a 2D model, this agrees well with the data point in Figure 4(d), where $B = -12 \cdot 10^{-10} \text{ m}^{-1}$ when the BiO-SrO and vacuum barrier heights are both 3 eV, and the width of the combined barrier is 0.8 nm.

VII. ACKNOWLEDGEMENTS

This work forms part of a long-standing collaboration with J.W. Loram and J.L. Tallon who have provided key insights and suggestions at all stages. Helpful suggestions were received from C. Bergemann, who also supplied the PDE program, and T. Benseman.

* Corresponding author; email address: jrc19@cam.ac.uk

¹ K.H. Lang, V. Madhavan, J.E. Hoffman, E.W. Hudson, H. Eisaki, S. Uchida and J.C. Davis, *Nature (London)*, **415**, 412 (2002).

² K. McElroy, Jinho Lee, J.A. Slezak, D.-H. Lee, H. Eisaki, S. Uchida and J.C. Davis, *Science*, **309**, 1048 (2005).

³ J. Bobroff, H. Alloul, S. Ouazi, P. Mendels, A. Mahajan, N. Blanchard, G. Collin, V. Guillen, and J.-F. Marucco, *Phys. Rev. Lett.* **89**, 157002 (2002).

⁴ J.W. Loram, J.L. Tallon and W.Y. Liang, *Phys. Rev. B* **69**, 060502(R) (2004).

⁵ E.L. Wolf, Chapter 2, *Principles of Electron Tunneling Spectroscopy* (Oxford University Press, Oxford, 1985).

⁶ J.Y.T. Wei, C.C. Tsuei, P.J.M. van Bentum, Q. Xiong, C.W. Chu and M.K. Wu, *Phys. Rev. B* **57**, 3650 (1998).

⁷ W.E. Pickett, *Rev. Mod. Phys.* **61**, 433 (1989).

⁸ G. Kinoda, T. Hasegawa, S. Nakao, T. Hanaguri, K. Kitazawa, K. Shimizu, J. Shimoyama and K. Kishio, *Phys. Rev. B* **67**, 224509 (2003).

⁹ R.M. Hazen in *Physical Properties of High Temperature Superconductors II* (World Scientific, Singapore, 1990), D.M. Ginsberg (Ed.), pages 121-198.

¹⁰ T. Watanabe, T. Fujii and A. Matsuda, Phys. Rev. Lett., **79**, 2113 (1997).

¹¹ V. M. Krasnov, A. Yurgens, D. Winkler, P. Delsing, and T. Claeson, Phys. Rev. Lett. **84**, 5860 (2000).

¹² FlexPDE 3, PDE Solutions Inc. Antioch, CA.

¹³ L.I. Schiff, Chapter V *Quantum Mechanics* (McGraw-Hill, New York,1955).

¹⁴ Using the syntax of “FlexPDE 3”, the BCs on all non-vertical straight lines in Fig.1 were Natural(ψ_R) and Natural(ψ_I) = 0, i.e. normal derivatives were set to zero there. The BCs on all vertical lines except the STS tip were NOBC(ψ_R) and NOBC(ψ_I), i.e. no BCs were applied there, nor were any applied to the small circles representing the O²⁻ ions. The BC on the STS tip representing an incoming wave at an angle θ to the normal is explained in the text. The BCs on the large semi-circular bounding region were Natural(ψ_R) = $-\frac{2\pi}{\lambda}\psi_I$ and Natural(ψ_I) = $\frac{2\pi}{\lambda}\psi_R$ representing an outgoing wave. The BCs on the small arc of the STS tip were the same but with $\frac{2\pi}{\lambda}$ replaced by k_F^{Au} .

¹⁵ F. W. Schmidlin, Journ. Appl. Phys. **37**, 2823 (1966). Note that in this work the barrier height is *decreased* by *positively* charged ions.

¹⁶ R.C. Dynes, V. Narayanamurti and J.P. Garno, Phys. Rev. Lett. **41**, 1509 (1978).

¹⁷ S.H. Pan, J.P. O’Neal, R.L. Badzey, C. Chamon, H. Ding, J.R. Engelbrecht, Z. Wang, H. Eisaki, S. Uchida, A.K. Gupta, K.-W. Ng, E.W. Hudson, K.M. Lang and J.C. Davis, Nature (London) **413**, 282 (2001).

¹⁸ Jinho Lee, K. Fujita, K. McElroy, J.A. Slezak, M. Wang, Y. Aiura, H. Bando, M. Ishikado, T. Masui, J.-X. Zhu, A.V. Balatsky, H. Eisaki, S. Uchida and J.C. Davis, Nature (London) **442/3**, 546 (2006).

¹⁹ G.E. Blonder, M. Tinkham and T.M. Klapwijk, Phys. Rev. B **25**, 4515 (1982).

²⁰ S. Kashiwaya, Y. Tanaka, M. Koyanagi, and K. Kajimura, Phys. Rev. B **53**, 2667 (1995).

²¹ T. Cren, D. Roditchev, W. Sacks, J. Klein, J.-B. Moussy, C. Deville-Cavellin and M. Lagu  s, Phys. Rev. Lett. **84**, 147 (2000).

²² J.W. Loram, K.A. Mirza, J.R. Cooper and J.L. Tallon, J. Phys. Chem. Solids **59**, 2091 (1998).

²³ H. Ding, T. Yokoya, J. C. Campuzano, T. Takahashi, M. Randeria, M. R. Norman, T. Mochiku, K. Kadowaki, J. Giapintzakis, Nature **382**, 51 (1996).

²⁴ D.S. Marshall, D.S. Dessau, A.G. Loeser, C.-H. Park, A.Y. Matsuura, J.N. Eckstein, I. Bozovic, P. Fournier, A. Kapitulnik, W.E. Spicer and Z.-X. Shen, Phys. Rev. Lett. **76**, 4841 (1996).

²⁵ Ch. Renner, B. Revaz, J.-Y. Genoud, K. Kadowaki, and   . Fischer, Phys. Rev. Lett. **80**, 149 (1998).

²⁶ B.W. Hoogenboom, K. Kadowaki, B. Revaz and   . Fischer, Physica C **376-380**, 15 (2003).

²⁷ J. Tersoff and D.R. Hamann, Phys. Rev. B **31**, 805 (1985)